This is the Pre-Published Version.
H. Niu, C. Chen, Y. Liu, L. Li, Z. Li, D. Ji, X. Huang (2022) *Mitigating Thermal Runaway Propagation of NCM 811 Prismatic Batteries via Hollow Glass Microspheres Plates*, **Process Safety and Environmental Protection**, https://doi.org/10.1016/j.psep.2022.04.049

Mitigating Thermal Runaway Propagation of NCM 811 Prismatic Batteries via Hollow Glass Microspheres Plates

Huichang Niu[a,*], Caixing Chen[a], Yanhui Liu [b,*], Lei Li[a], Zhao Li[a], Dan Ji[a], Xinyan Huang [b,c,*]

[a] *Guangzhou Institute of Industrial Technology, Guangzhou, China*

[b] *Research Center for Fire Safety Engineering, The Hong Kong Polytechnic University, Hong Kong, China*

[c] *The Hong Kong Polytechnic University Shenzhen Research Institute, Shenzhen, China*

* Corresponding to xy.huang@polyu.edu.hk for any inquiry

Abstract: The propagation of thermal runaway in Lithium-ion battery module can escalate fire hazards and damage in energy storage systems. More effective strategies are needed to ensure the safe application of high-energy lithium-ion batteries and alleviate the thermal runaway propagation. This work explores the use of the ultra-light plates based on hollow glass microspheres (HGM) as firewalls in the large-format battery module. A systematic experimental study is conducted using the prismatic battery with $LiNi_{0.8}Co_{0.1}Mn_{0.1}O_2$ (NCM 811) cathode and HGM firewalls with different thicknesses. Performance tests suggest that the composite plate with 60 wt.% HGM, 25 wt.% curing agent, and 15 wt.% flame retardant is most effective in mitigating thermal runaway propagation. Without firewalls, the thermal runaway propagation rate increases from 0.43 cell/min to 0.85 cell/min as the SOC level increases from 25% to 100%. Inserting HGM plates can effectively slow down thermal runaway propagation, where the 3-mm HGM plates can successfully block the thermal runaway. A simplified heat transfer model is also proposed to explain the performance of firewall on inhibiting thermal runaway and help to optimize the safety design for battery modules. This work provides important insights into the thermal runaway risks and safety measures of large battery systems.

Keywords*: battery safety; composite plate firewall; fire protection; thermal insulation plate; propagation rate.*

1. Introduction

Lithium-ion batteries (LIBs) have been perceived as promising power sources and energy storage devices owing to high energy density, long cycle life, and environmental friendliness [1] . However, the active and flammable components in LIBs make them inherently vulnerable to fire and explosions, so their safety issue poses a severe challenge to their application and development [2–4]. The thermal runaway initiated by external abuse or internal flaws can rapidly heat the battery, release flammable gases, and inject flames [5]. Once a cell goes thermal runaway, the released heat can easily propagate to the adjacent cell and trigger the cascading failure within the battery module, elevating the fire hazards exponentially and leading to an explosion [6,7]. Therefore, inhibition of the thermal runaway propagation is of great significance to ensure the safety of battery-based energy storage systems.

Mitigating the thermal runaway propagation over the LIB module is an emerging research topic, where the corresponding strategies could be classified into four categories, i.e., prevention, detection,

© 2022 This manuscript version is made available under the CC-BY-NC-ND 4.0 license http://creativecommons.org/licenses/by-nc-nd/4.0/

compartmentation, and suppression [8,9]. The purpose of prevention is to avoid thermal runaway, such as promoting LIB intrinsic safety [10] and optimizing the thermal management systems of the battery modules [11,12]. For example, Yang et al. (2022) developed a film-forming flame-retardant additive for the $LiNi_{0.8}Co_{0.1}Mn_{0.1}O_2$ (NCM 811) cathode to promote battery safety performance. Dai et al. (2022) improved the flame retardancy of the conventional phase change materials (PCM) and employed them to mitigate the thermal runaway of cylindrical batteries. The early detection aims to warn of the potential fire risk in LIB systems where the characteristic signals, such as temperature, voltage, and gas composition, within the battery systems, are monitored and detected in real-time [13–16]. After the occurrence of thermal runaway, the passive compartmentation strategy based on thermal insulation materials is essential to restrict the thermal runaway propagation [17,18]. The fire suppression technology should be activated to extinguish the flame and cool down the battery cells [19–24].

Large-format LIB has a high inherent fire hazard, especially for the LIB with NCM 811 as the cathode material (Liu et al., 2022). The thermal runaway propagation of large-format LIBs is primarily driven by cell-to-cell heat conduction through the contact area, where 12% of the total heat released by a failed cell is enough to initiate the thermal runaway of the adjacent cell [26]. Thus, using interstitial material as the thermal barrier is one of the most cost-effective countermeasures for thermal runaway propagation within LIB modules, and it has been investigated extensively [4,27]. For example, Feng et al. (2015a) found that materials with a thickness of at least 1 mm and a thermal conductivity of less than 0.2 W/(m-K) can achieve good insulation performance to block thermal runaway propagation within a large format LIB module. Li et al. (2021) proposed a 1-mm-thick smart firewall consisting of a non-flammable phase change material (NFPCM) and a silica nanofiber. When a cell undergoes a high temperature, the NFPCM stored in the firewall will absorb heat and change phase, whereas the remaining silica nanofibrous mats with the low thermal conductivity of 0.026 W/(m-K) can quench the thermal runaway propagation. Rui et al. (2021) inserted aerogel pads into the prismatic LIB module with the liquid cooling system and validated its efficacy in preventing thermal runaway propagation. Moreover, the phase change material (PCM)-based firewalls were also developed to alleviate the thermal runaway propagation [12,31,32]. However, the weight of PCM- based firewalls is still a big issue that significantly affects the energy density of entire LIB module. And the literature lacks sufficient experimental data to validate the practicability of compartmentation strategies for mitigating thermal runaway propagation in the $LiNi_{0.8}Co_{0.1}Mn_{0.1}O_2$ based LIB module. Therefore, industrial communities are still calling for more thermal barriers with low density and cost advantages for the fire safety of high-energy LIB systems.

The hollow glass microsphere (HGM) is a rigid inorganic spheric particle, containing more than 90% silica. Featured by lightweight, low thermal conductivity, high compressive strength, and electrical insulation, HGM has been widely used in building materials, aerospace, and coatings [33]. When mixed with epoxy, hollow glass microsphere-based materials could be prepared with different shapes and sizes. Therefore, it can be an excellent firewall in LIB modules to prevent thermal runaway propagation. To the best of our knowledge, little work has explored the feasibility of HGM based material on inhibiting battery fire propagation, especially for its application in the $LiNi_{0.8}Co_{0.1}Mn_{0.1}O_2$ based LIB module.

This work manufactures ultra-light hollow glass microsphere (HGM) plates for thermal runaway

propagation mitigation. By changing the component ratios and conducting standard tests, a typical HGM plate with low thermal conductivity, excellent fireproof performance, and high compressive strength is selected as the firewall within LIB modules. A series of tests are implemented on LIB modules with $LiNi_{0.8}Co_{0.1}Mn_{0.1}O_2$ (NCM811) as cathode material to comprehensively investigate the effects of the state of charge (SOC) and HGM plate thickness on thermal runaway propagation characteristics. The thermal and toxic hazards are also analyzed, which would be helpful to deal with the problems of environmental pollution caused by the battery fire. Moreover, a simplified heat transfer model is proposed to explain how the firewall slow down and prevent the thermal runaway propagation in batteries.

2. Experimental Methods

2.1 Production of HGM plates

The HGM plate is prepared as the thermal barrier to inhibit the thermal runaway propagation within the battery module, which is made of three major components, including row material (HGM), fire retardant (FR), and the binding agent (BA). The substrate HGM plays the role of thermal insulation, accounting for the highest mass ratio. FR aims to improve the flame-retarded property and compose Ammonium Polyphosphate (APP) and Dipentaerythritol (DPE) in the mass proportion of 2:1. The BA contains epoxy and amine curing agents with a mass ratio of 3:1, which can improve the mechanical properties and chemical resistance of HGMP. The selected epoxy resin E51 was purchased from Shanghai Macklin Biochemical Co., Ltd (E871957). According to the specification, it has an epoxy value ranging from 0.48-0.54 mol/100g and the viscosity (25 °C) ranging from 9000-14000 Mpa-s.

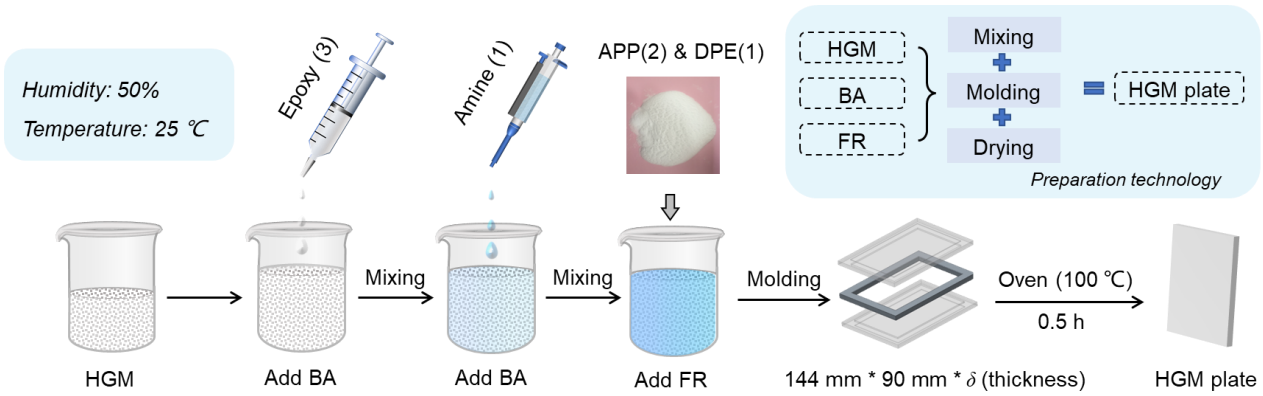

Fig. 1. The preparation procedures of hollow glass microsphere (HGM) plate with fire retardant (FR) and the binding agent (BA).

The detailed preparation procedures of the HGM plate are illustrated in Fig. 1, and the preparation process was conducted under the ambient temperature of 25 °C and the relative humidity of 50%. The substrate HGM was firstly mixed with epoxy, and then an amine curing agent with the quality of one-third of epoxy resin was added. After sufficient stirring, the homogeneous mixture of HGM and BA was mixed with FR material (i.e., the mixture of APP and DPE with the mass ratio of 2:1). The purpose of adding FR at the end allowed it to cover the surface and enhance the flame-retardant performance. After perfectly stirring, the mixture was poured into the mold and dried in an oven with a constant temperature of 100 °C for 0.5 h. Finally, the HGM plate

with a length of 144 mm and a width of 90 mm was successfully manufactured.

Table 1. Mixture proportions of hollow glass microsphere (HGM), fire retardant (FR), and the binding agent (BA).

HGM Plate No.	HGM (wt.%)	FR (wt.%)	BA (wt.%)
HGM-1	50%	25%	25%
HGM-2	50%	20%	30%
HGM-3	50%	15%	35%
HGM-4	60%	20%	20%
HGM-5	60%	15%	25%
HGM-6	60%	10%	30%
HGM-7	70%	15%	15%
HGM-8	70%	10%	20%
HGM-9	70%	5%	25%

The manufactured HGM plate can exhibit different behaviors in thermal insulation, fire retardancy, and mechanical stability under the different mixing proportions of HGM, FR, and BA. Nine mixture proportions were selected for HGM plate preparation, as listed in Table 1. Three standard tests were adopted in this study to characterize the performance of thermal insulation, fire retardancy, and mechanical stability. The thermal conductivities of HGM plates were measured by the Hot Disk transient plane source technique (TPS 2200, Sweden), where the sample was cut as a cylinder with a diameter of 30 mm and a thickness of 5 mm.

Flame-retardant properties of the HGM plate were determined by the UL-94 vertical combustion test. Samples with the size of 125 mm×13 mm×10 mm were vertically arranged and ignited by a flame for 10 s and for two times. Particularly, V-0 is considered the best class where the flame can self-extinguish within 10 seconds after the first 10-second fire ignition and within 30 s after the second fire ignition. Furthermore, the cone calorimeter (ISO 5660) is another powerful method to test the fire behavior of the objects, which can provide the radiative heating condition and determine the heat release rate and heat of combustion of objects [34,35]. In the real application, HGM plates are inserted between cells, so that the radiative heating during thermal runaway could not play a dominant role to damage the HGM plates. Referring to the previous study [36], the HGM plates were tested under a constant external heat flux of 25 kW/m^2.

Mechanical properties of the samples (Φ 40 mm×15 mm) were analyzed by the compression test, which is supported by a universal electronic material testing machine (MTS/Insight 50 kN) with a loading rate of 2 mm/min. Comprehensively considering the thermal, fire-retardant, and mechanical properties of HGM plates, the most optimal HGM plate would be selected to block the thermal runaway propagation within LIB modules in the tests.

2.2 Battery samples and test setup

Commercial prismatic LIBs (2514490, Contemporary Amperex Technology Co., Limited) with a nominal capacity of 51 Ah and a nominal voltage of 3.70 V were selected in this work. The cathode material of this LIB is $LiNi_{0.8}Co_{0.1}Mn_{0.1}O_2$ (NCM 811), which is anticipated as the promising cathode candidate for the next-generation LIBs but has relatively high risks (Wang et al., 2021). The anode material is the graphic carbon.

The ceramic-coated polypropylene–polyethylene (PP) is used as the separator inside the battery. In terms of electrolyte, the lithium salt is $LiPF_6$, and the organic solvent is the mixture of ethylene carbonate (EC) and dimethyl carbonate (DMC) and ethyl methyl carbonate (EMC) with specific combustion heat of 12.38 and 18.41 MJ/kg [35,38].The weight of the LIB sample is 817±2 g, and its theoretical energy density can exceed 260 Wh/kg.

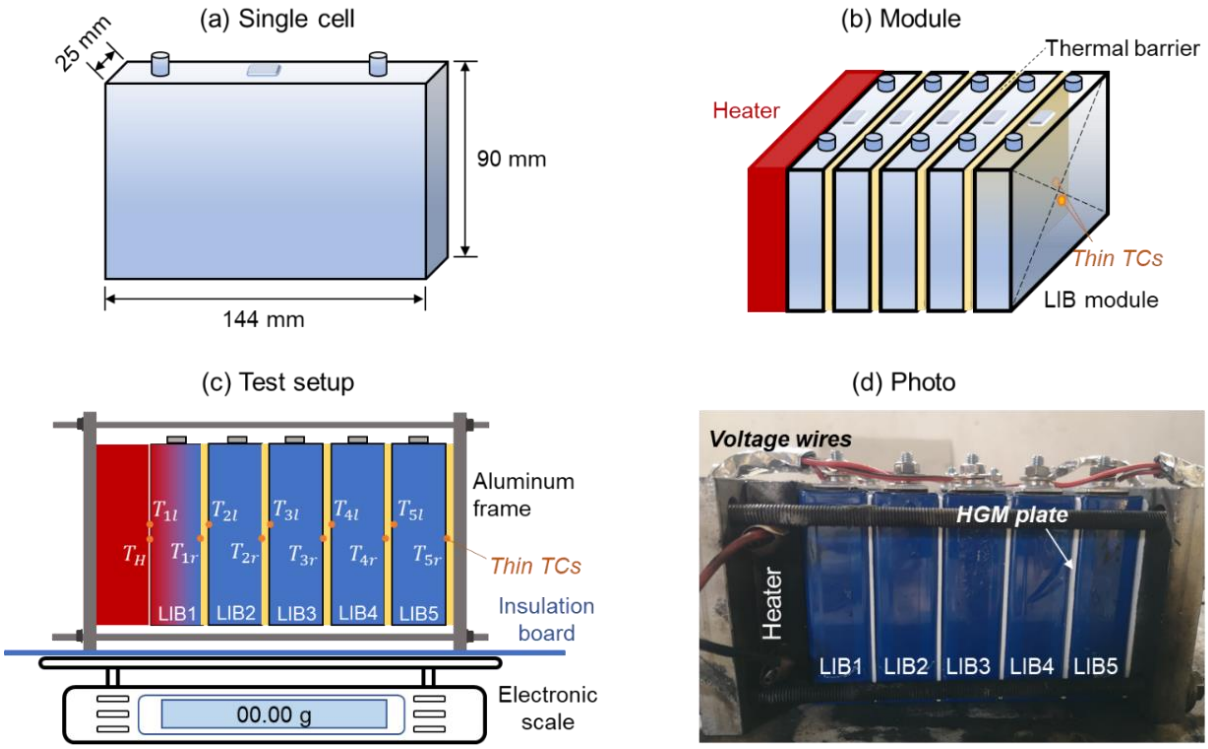

Fig. 2. Schematic diagram of (a) LIB sample, (b) LIB module, and (c) experimental setup; (d) photograph of LIB module before the side-heating test (with HGM plate case).

As illustrated in Fig. 2a, the LIB cell has a height of 90 mm, a length of 144 mm, and a thickness of 25 mm. To reduce the experimental uncertainty, LIBs from the same manufacturing batch were used in this study. Five prismatic cells are manually assembled into a linear LIB module, as shown in Fig. 2b. Within the LIB module, four thermal barriers were inserted between cells to prevent the thermal runaway from propagation. To initiate a uniform and consistent thermal runaway, an electrical heater (144 mm × 90 mm × 25 mm) made of aluminum was employed to simulate a thermal-failed cell and trigger the thermal runaway of the first cell (i.e., LIB1). Referring to the Electric Vehicles Traction Battery Safety Requirements released by China (GB 38031) [39], constant heating power of 900 W was selected in this work. The surface temperatures of both heater and cells were monitored by the K-type thermocouples with a fine bead diameter of 0.25 mm (Omega Engineering Limited). To acquire accurate temperature information, thermocouples were attached on the two sides of cells near the central surface. As demonstrated in Fig. 2b, thermocouples attached to the left surface of LIBs were 10 mm higher than thermocouples attached to the right surface of LIBs in all tests.

The aluminum frame was used to hold the heater and five parallel cells to ensure close contact between cells (Fig. 2c), and the mass evolution of the LIB module was recorded by an electronic balance with the data acquisition frequency of 10 Hz (GX-10K, A&D Company, Limited). During the entire test, several electrical

wires were used to monitor the voltage information of each cell (Fig. 2d). The real-time temperature and voltage information was collected by the data logger (HIOKI LR8400) per second throughout the test. A digital camera (SONY FDR-AX40, 25 fps) was employed to record the thermal runaway propagation behaviors and fire processes. After each test, the particles vented from batteries were collected from papers on the ground within a distance of 4 m from the center of the module.

2.3 Test procedures and controlled parameters

As illustrated in Fig. 2c and Fig. 2d, a 900-W heater was used to trigger the thermal runaway propagation of LIB modules. Once the thermal runaway of LIB1 was initiated, the heater was turned off. During the thermal runaway propagation tests, two key parameters were controlled for a given HGM formula:

(I) Battery SOC level. Five SOC values of 0%, 25%, 50%, 75%, and 100% were selected for all NCM 811 cells in the module. The SOC calibration was conducted with the aid of a battery cycler made by Neware (BTS-4000). Before the test, all cells were first charged to 4.2 V with a constant current of 25.5 A, and then charged under the constant voltage of 4.2 V until the current decreased to 2.55 A. Afterwards, batteries were brought to the desired SOC level with the discharge current of 51 A. After the charging/discharging process, all cells rested at least 2 h to minimize the heating effect during the cycling.

(II) The thickness of the HGM plate (δ). As it is difficult to manually prepare the HGM plate with a thickness less than 1.5 mm, HGM plates with thicknesses of 1.5 mm, 2 mm, and 3 mm were manufactured in this study and then examined for the thermal runaway propagation tests.

All experiments were conducted under the ambient temperature of 30 ± 2 °C. For each case, at least two repeating tests were conducted to reduce the random error. Since the toxic emissions of the battery fire can pose a significant threat to environmental safety [9], the venting particles of the LIBs after thermal runaway were collected and underwent chemical analysis. The Scanning Electron Microscope (SEM–JSM7800 F, JEOL) and Energy Dispersive X-Ray Spectroscopy (EDS JSM7800 F, JEOL) were employed to investigate the SOC effect on surface micromorphology and element composition of these particles.

3. Results and Discussions

2.4 Properties of the HGM plates

Aiming to mitigate thermal runaway propagation within high-energy LIB systems, the firewalls should behave with low thermal conductivity, suitable anti-press properties, and excellent fireproof performance. To select the most optimal material for firewalls, nine kinds of HGM plates with different component ratios were manufactured and underwent the hot-Disk test, compression test, and UL-94 combustion test. Results of the above tests and overall evaluation are summarized in Fig. 3.

Thermal conductivity is the most significant parameter to evaluate the thermal insulation performance of HGM plates. As shown in Fig. 3a, thermal conductivity value ranges from 0.058 W/m-K to 0.070 W/m-K, much lower than the threshold value (i.e., 0.2 W/m-K) for thermal conductivity of interstitial material proposed by Feng et al. (2015a). Thus, the thermal insulation property of prepared HGM plates is good enough to block thermal runaway and prevent its propagation within LIB modules. The swelling of failed LIB may lead to a

compression force between cells and destroy firewalls, the compressive strength is vital for HGM plates to maintain their performance. Fig. 3b shows the compressive strength of prepared HGM plates ranges from 0.81 MPa to 2.06 MPa, where its strength increases with both factions of HGM and BA. For large-format pouch cells, the compression force between cells can reach 445 N during the thermal runaway process [13]. Then, the equivalent pressure for cells in this work is about 0.034 MPa, which is much lower than the limiting strength of prepared HGM plates.

In terms of fireproof performance, Fig. 3c summarizes the flaming time of HGM plates under the UL-94 vertical burning test. It is apparent that the self-extinguishing characteristics of all samples can meet the UL94 V-0 flame-retardant standard. That is, the flaming time exists less than 10 s after the 1st ignition and less than 30 s after the 2nd ignition. Moreover, the results of cone tests showed that all HGM plates were difficult to ignite. Therefore, HGM plates prepared in this work are eligible to serve as the firewalls within LIB modules.

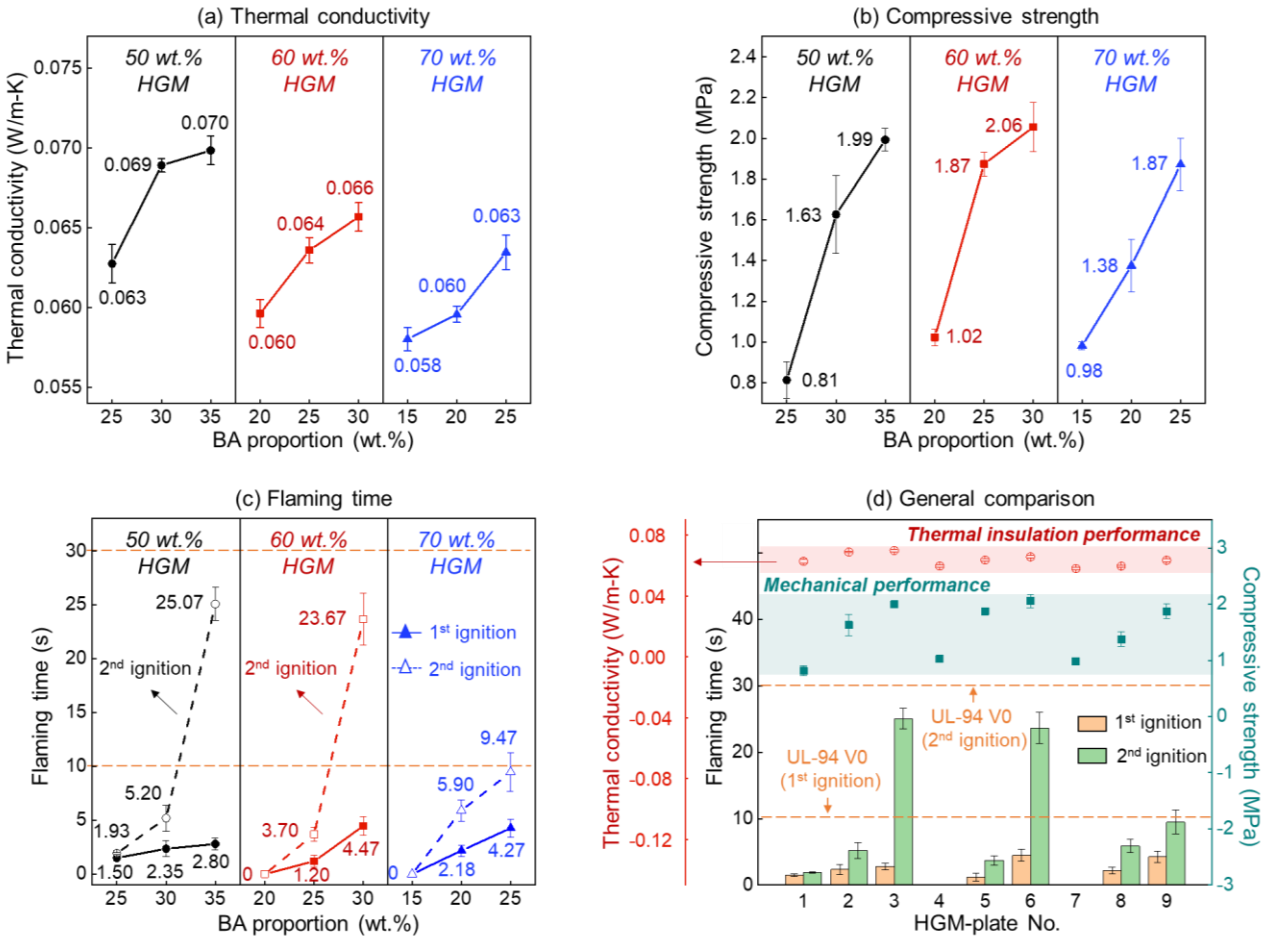

Fig. 3. (a) Thermal conductivities of HGM plates with different component ratios, (b) compressive strengths of prepared HGM plates in the compression test, (c) flaming time of HGM plates in UL-94 vertical combustion test, and (d) overall comparison on thermal, mechanical, and flammability properties of HGM plates.

To further select the optimal firewall for thermal runaway propagation prevention, Fig. 3d comprehensively compares the thermal, mechanical, and flammability properties of prepared HGM plates. It is evident that the thermal conductivities of HGM plates are similar, around 0.064 ± 0.004 W/m-K. But there are significant differences in the mechanical and flammability properties of different HGM plates. Specifically,

HGM-3 and HGM-6 behave the highest compressive strength, while their flaming durations in the UL-94 test are long and indicate the relatively low-fireproof performance. HGM-4 and HGM-7 have the best fire-resistant properties, while their compressive properties are relatively poor. Finally, HGM-5 can be perceived as the most suitable firewall for the following thermal runaway propagation test. It has a density of 0.086 g/cm^3, a thermal conductivity of 0.064 W/m-K, and a compressive strength of 1.87 MPa. The detailed parameters of this plate are listed in Table 2.

Table 2. Properties of selected HGM plates for thermal runaway propagation tests

Component ratios (HGM: FR: BA)	Density (g/cm^3)	Thermal conductivity (W/m-K)	Compressive strength (MPa)	Fire retardancy level
60%: 15%: 25%	0.086	0.064	1.87	UL-94 V0

2.5 Thermal runaway propagation

As a baseline, the fire hazards of LIB modules without firewalls are first presented under different SOCs. Fig. 4 shows the snapshots of the thermal runaway propagation at 100% SOC and 25% SOC modules without firewalls, where the thermal runaway of LIBs occurred in succession. As shown in Fig. 4a, the fully charged LIB module was initially heated by the electrical heater. During the heating, the exothermic chain reactions inside the LIB were induced and further increased the LIB temperature. At around 8 min, the LIB1 reached thermal runaway, accompanied by considerable sparks and flammable gases. The spark thereby ignited the combustible gases, and the jet flame was formed. For prismatic LIB with relatively low energy density in literature, the flame jet only occurred near the safety valve [40,41]. Interestingly, multiple flame jets in this work happened from both the safety valve and LIB surface. This is because the heat generated by the thermal runaway melted the aluminum shell of the LIB, and flammable gas was ejected from the gap and caught violent fire (Video S1). Afterward, LIB 2-5 successively failed, where the high-temperature gases and material emitted from LIB with a high velocity, resulting in the flame lift.

For LIBs with 25% SOC (Fig. 4b), there was no flaming combustion during the thermal runaway process of the LIB with 25% SOC (Video S2), where the intense combustion was replaced by a large amount of smoke. Both the thermal runaway time of LIB1 and the entire thermal runaway propagation duration of low-SOC were significantly prolonged, similar to the thermal runaway propagation tests of NCM 111 LIB modules [42,43].

Fig. 4. Photos of thermal runaway propagation (TRP) within LIB modules at (a) 100% SOC and (b) 25% SOC.

Fig. 5a shows the evolution curves of mass, voltage, and temperature for the LIB module with 100% SOC during the thermal runaway propagation test. In the beginning, the total weight of the LIB module and aluminum frame is 8.6 kg, and the initial voltages of LIBs are all around 4.18 V. Under the side heating, the thermal runaway process of a large format LIB can be classified into four stages: (I) heating, (II) failure, (III) transition, (IV) thermal runaway. The left-surface temperature of LIB1 (T_{1l}) elevates at an average rate of 0.45 °C/s during the heating stage. At 474 s, the value of T_{1l} rapidly increases at approximately 71 °C/s, indicating the occurrence of the local thermal runaway near the left surface of LIB1. At this moment, the right-surface temperature of LIB2 (T_{1r}) is only 71 °C, and the voltage starts to drop due to the large-scale internal short circuit.

At 482 s, the steep increase of T_{1r} and the decreasing of voltage suggest that the whole LIB1 reaches thermal runaway drastically, accompanied by a large number of sparks ejected and smoke released. Due to the reaction force of the gas ejection, the LIB module mass has a short rise and then drops to 8.16 kg sharply. Since the transition time from local failure to the whole thermal runaway is very short (~ 8 s), the thermal runaway onset time of LIB1 can be regarded as the average onset time of these two thermal runaway events. Under the heating effect of failed LIB1, the thermal runaway of other LIBs sequentially occurs within the module (Fig. 5a) and lasts for about 5 min. The average thermal runaway propagation time from one cell to the adjacent cell $\overline{\Delta t}$ is about 1.3 min. Finally, the total mass of LIB module drops to 6.65 kg, and the average mass loss of a single cell $\overline{\Delta m}$ is about 0.39 kg.

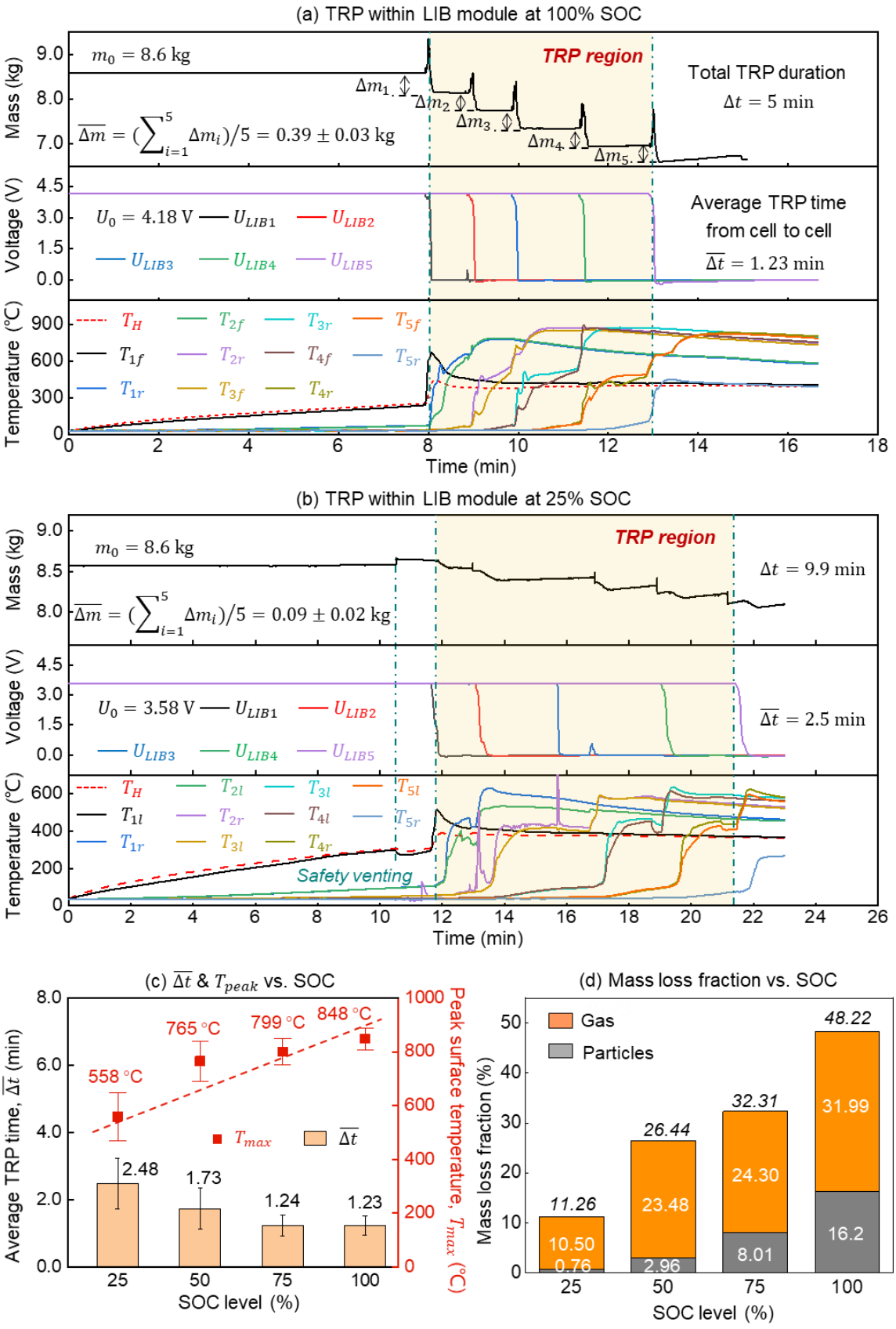

Fig. 5. Evolution curves of mass, voltage, and temperature for LIB modules with (a) 100% SOC and (b) 25% SOC; SOC levels varying with (c) average thermal runaway propagation (TRP) time from one cell to adjacent cell, peak surface temperature of LIBs, and (d) mass loss fraction of LIBs.

The variations of mass, voltage, and temperature for the 25% SOC LIB module during the thermal runaway propagation test are summarized in Fig. 5b, where a similar cascading-failure behavior is observed. Since a lower amount of electrochemical energy is stored in cells with 25% SOC, the thermal runaway reactions inside the LIB are relatively mild, and the temperature increase rate at the heating stage is lower than 0.38 °C/s. Interestingly, the gas venting of LIB1 is captured by mass and temperature curves where a slight mass increase and a temporary temperature decrease appear at 631 s. Furthermore, the onset time for LIB1 thermal runaway is significantly delayed by 3.7 min compared with that in the 100% SOC module, and the thermal runaway propagation duration is also prolonged to 9.93 min in the 25% SOC module.

The average temperature of 25% SOC LIBs after thermal runaway is about 200 °C lower than that of 100% SOC LIBs, which could be insufficient to ignite the flammable gases. Therefore, no sparks and flaming combustion are observed during the thermal runaway propagation process (Fig. 4b). For LIBs at 0% SOC, although the gas venting of LIB1 occurs and the voltage of LIB1 eventually reaches 0, the LIB1 does not undergo the thermal runaway. In this case, the current of the heater was cut off until the venting of LIB2. After turning off the heater, the temperature of LIB1 and LIB2 decreased, and no thermal runaway propagation happened (see Fig. S1 in Supplementary materials).

To clarify the SOC effect on thermal runaway propagation characteristics, Fig. 5c compares the average thermal runaway propagation time from one cell to the adjacent cell $\overline{\Delta t}$ and peak surface temperature T_{peak} of LIB modules with different SOC levels. Apparently, the value of $\overline{\Delta t}$ decreases with SOC level, which suggests that thermal runaway is prone to propagate within the high-SOC LIB module. Specifically, the decrement of average thermal runaway propagation time is 49.2% as the SOC increases from 25% to 100%. Moreover, SOC level also has an important influence on the peak surface temperature of LIBs during thermal runaway (T_{max}). The left surface temperature of LIB1 (T_{1l}) is affected by the heater, so that this value is not considered in Fig. 5c. As expected, the value of T_{max} increases from 558 °C to 848 °C as the SOC increases from 25% to 100%. Compared with the research findings in previous works [44], the maximum surface temperature of NCM 811 LIB during thermal runaway is much higher than that of LIBs with NCM 111, NCM 523, and NCM 622 as cathode materials, exhibiting a higher fire risk.

The original mass of the battery module is about 8.6 kg, including five LIBs (about 0.817 kg per cell), an electrical heater, and the supporting frame. After the thermal runaway propagation tests, the masses of LIB residues and ejected particles are measured, and the mass losses via gases are accordingly calculated. As shown in Fig. 5d, the mass loss fraction for LIBs at 100%, 75%, 50%, and 25% are 48.22%, 32.31%, 26.44%, and 11.26%, respectively. Thus, a higher SOC level leads to a more mass loss after the thermal runaway, agreeing with more ejection of gases and particles observed in the experiment. Moreover, both mass losses via gases and particles increase with SOC level, which validates that the high-SOC LIBs have high thermal hazards and toxic hazards. Remarkably, the particulate emission increases by over 20 times as the SOC increases from 25% to 100%. Given that particles emitted from thermal runaway of Ni-rich LIBs are very toxic to the human body [45], it is of great significance to further investigate the characteristics of these particles.

After the thermal runaway propagation tests, the venting particles of the LIBs are carefully collected and prepared for the SEM/EDS analysis. A 0.5k magnification is used to characterize the entire surface morphology

and composition of vent particles, and the SEM/EDS results are summarized in Fig. 6. From the SEM observation, it is evident that the vent particles mainly consist of spherical shapes and irregular bulk shapes. The diameters of most spherical particles are less than 30 μm, whereas the characteristic lengths of most particles with irregular bulk shapes are greater than 36 μm. For spherical particles, the major elements are carbon (C), oxygen (O), fluorine (F), manganese (Mn), cobalt (Co), nickel (Ni). Particularly, the large proportion of element Ni in spherical particles (~52%) suggests that these spherical particles primarily come from the thermal runaway reactions related to cathode materials. Thus, the metal elements can be extracted from these spherical particles from the perspective of LIB recycling.

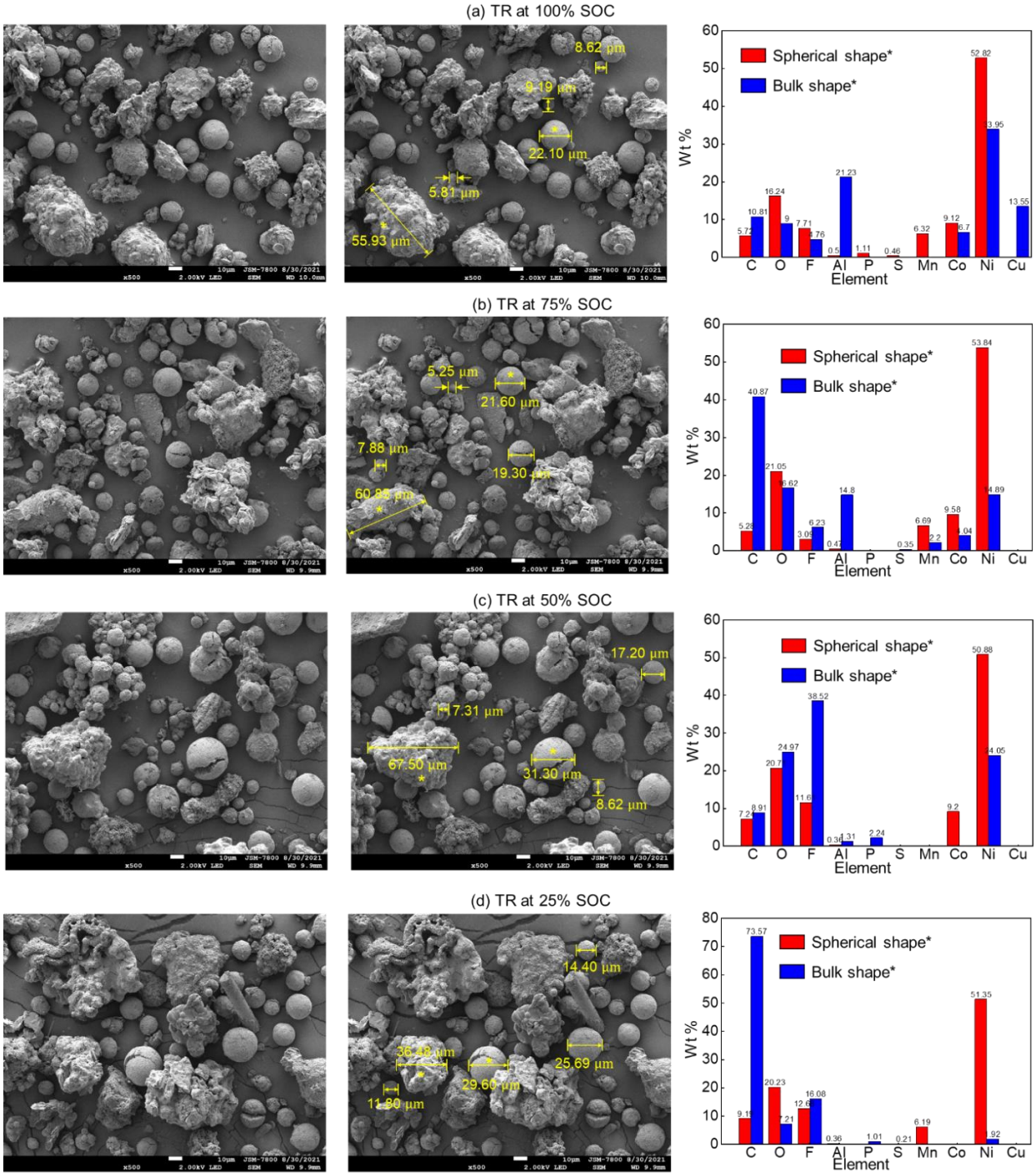

Fig. 6. SEM/EDS results for the vent particles of the LIB modules with (a) 100% SOC, (b) 75% SOC, (c) 50% SOC, and (d) 25% SOC.

In terms of bulk particles, the masses of elements C and F account for a large percentage, indicating that these particles could be the products of reactions related to the electrolyte, binder, and anode materials. The copper (Cu), which is the main element of the negative collector, is only detected in venting particles from LIBs with 100% SOC (Fig. 6a). This further confirmed that the fully charged LIBs have a high fire hazard, and the internal temperature of LIB at 100% SOC should be higher than 1085 °C (the melt temperature of copper).

Moreover, elements such as aluminum (Al), sulfur (S), fluorine (F), and phosphorus (P) in venting particles are harmful to the human body and the environment. The element sulfur should come from battery additives [46], where the sulfur-based compounds are used as additives in facilitating solid-electrolyte interphase (SEI) formation. Therefore, it is necessary to treat the vent particles and assess the quality of air, water, and soil near the battery fire incidence after LIB thermal runaway to determine the impact on the environment.

2.6 Effect of firewall plate thickness

As discussed above, the LIBs with NCM 811 cathode material have much higher fire hazards than other Ni-poor LIBs in the literature. Therefore, the NCM 811 LIB module with 100% SOC can be regarded as an excellent case to validate the efficacy of prepared HGM plates on thermal runaway propagation mitigation. Fig. 7 summarizes the temperature variations of 100% SOC LIB modules without the HGM plate (i.e., 0 mm thickness), 1.5 mm, 2 mm, and 3 mm.

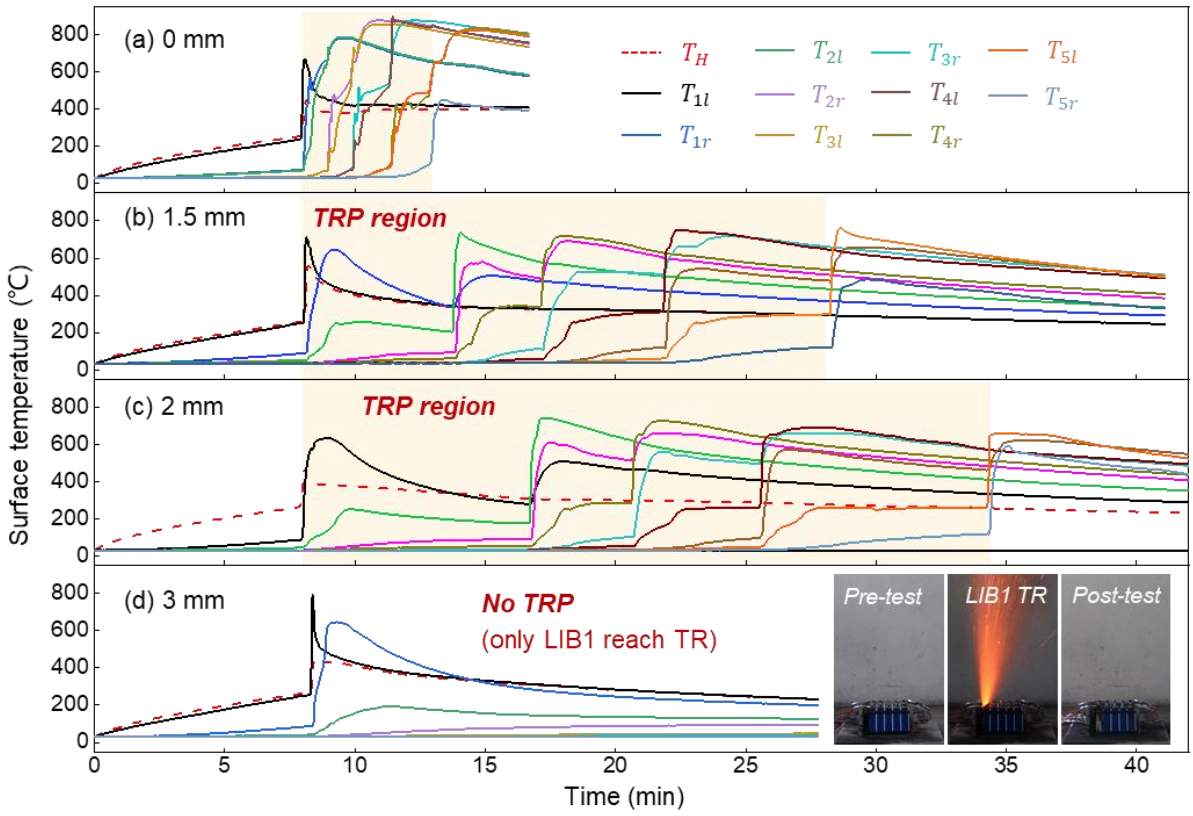

Fig. 7. Temperature variations and thermal runaway propagation (TRP) regions of 100% SOC LIB modules using HGM plates as firewalls with thicknesses of (a) 0-mm (no plate), (b) 1.5 mm, (c) 2 mm, and (d) 3 mm.

Since there is no firewall between the heater and LIB1, the thermal runaway onset time of LIB 1 is similar. However, inserting the HGM plates with the thickness of 1.5 mm and 2 mm, the thermal runaway propagation time can be prolonged to 20.2 min (Fig. 7b) and 26.4 min (Fig. 7c), compared with the 5-min duration of thermal runaway propagation without HGM plate in Fig. 7a. In other words, the rate of thermal-runaway propagation is significantly reduced by firewall plates. In particular, the 3-mm HGM plates can successfully stop the thermal runaway propagation (Fig. 7d). After the thermal runaway of LIB1, the left surface of LIB2 has a maximum temperature increase up to 180 °C while the maximum temperature of the right surface is lower than 90 °C. These two temperatures are much lower than the minimum surface temperature required for the thermal runaway in the Accelerating Rate Calorimeter (ARC) test, where the onset temperature for the thermal runaway of NCM 811 LIB should be higher than 240 °C. Therefore, most of the released heat from LIB1 thermal runaway is successfully insulated by the 3-mm HGM plates, which can prevent the thermal runaway propagation.

Except for HGM plates manufactured in this work, the aerogel pads [30] and phase change composite material with the flame retardant coating (FR-CPCM) [31] were used to prevent the thermal runaway propagation (TRP) of large format prismatic LIBs in literature. In the study conducted by Rui et al. (2021), 1-mm aerogel pads with thermal conductivity of 0.065 W/m-K were employed to mitigate the TRP of the NCM 111 battery. The heating power was 876.09 W, close to the heating power used in this work. Without firewalls, the TRP rate in NCM 111 module was around 4.5 times as fast as that in the LIB module with aerogel pads. In our work, the TRP rate in the no-HGM module is 4 times as fast as that in the LIB module with HGM plates. It should be noted that the thermal hazards of the NCM 811 battery are much higher than that of the NCM 111 battery. Thus, the mitigation effectiveness of HGM plates is effective.

Recently, Niu et al. (2022) employed the FR-CPCM to block the TRP of 40-Ah prismatic batteries. Results indicated that the 3-mm FR-CPCM plates could successfully prevent TRP from LIB-1 to LIB-2, where the maximum temperature of LIB-2 was around 182.6 °C. Similarly, the energy density of LIB in this work is higher so that the mitigation performance of the HGM plates could be better. In the future, this HGM plate can be collaborated with the liquid cooling method to ensure the safety of a high energy battery system. For example, the liquid cooling plate can be placed at the bottom of the battery module, and the synergistic effects of liquid flow rate and HGM thickness will be comprehensively investigated.

2.7 Heat transfer analysis

To further reveal the effect of SOC and HGM plate thickness on thermal runaway propagation characteristics, a mean thermal runaway propagation rate (or speed) from cell to cell, r [cell/min], is defined as

$$r = \frac{n}{\Delta t} \tag{1}$$

where Δt [min] is the thermal runaway propagation duration time; and n [cell] is the number of cells that goes thermal runaway during Δt. Therefore, r can be calculated from experimental data and summarized in Fig. 8.

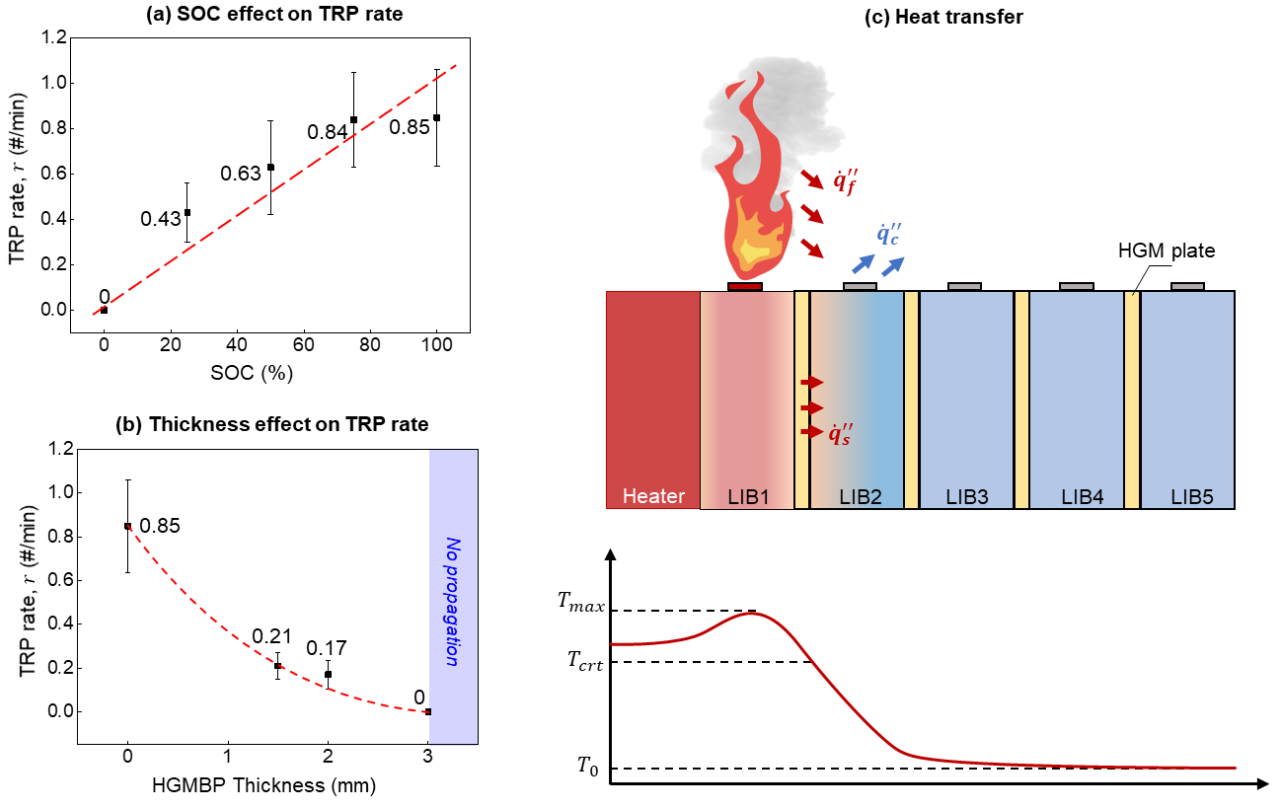

Fig. 8. (a) The thermal runaway propagation rate varying with the SOC level, (b) effect of HGM plate thickness on thermal runaway propagation rate within the 100% SOC LIB module, and (c) Schematic of thermal runaway propagation in a linear array of the LIB module (not to scale).

As shown in Fig. 8a, such a thermal runaway propagation rate increases with the increase of battery SOC. For example, the thermal runaway propagation is accelerated two times as the SOC increases from 25% SOC to 100% SOC, indicating the severe fire consequences for high-SOC LIB modules. Inserting HGM plates as firewalls, the thermal runaway propagation rate over a fully charged LIB module significantly decreases from 0.85 cell/min to 0 cell/min, showing the excellent inhibition efficacy of HGM plates (Fig. 8b).

In general, thermal runaway propagation is analogized to the fire spread, which can be regarded as a continuous ignition process of LIBs. The main driving force for thermal runaway propagation is the heat transfer between LIBs, while the thermal runaway propagation is resisted by the LIB thermal inertia (Fig. 8c). Thus, the thermal runaway propagation rate is controlled by the ratio of thermal runaway propagation driving force to the thermal inertia of LIBs [19,42], which can be expressed as

$$r \approx \frac{\text{Net heating rate}}{\text{Thermal resistence}} = \frac{\dot{q}_s + \dot{q}_f - \dot{q}_c}{m_{LIB} c_{LIB} (T_{crt} - T_0)} \tag{2}$$

where $\dot{q}_s$ is the effective heating rate through the surface of LIB2 shell; $\dot{q}_f$ is the heating contributed by flame or smoke of the failed cell (LIB1); $\dot{q}_c$ represents the environmental cooling rate; m_{LIB} is the density of the

LIB; c_{LIB} is the total heat capacity of the LIB, which is about 1100 J/kg-K in ARC test [47]; T_{crt} is onset temperature for thermal runaway, which is measured around 240 °C [47]; and T_0 is the ambient temperature, respectively.

For the failed cell (LIB1), the peak temperature after thermal runaway (T_{max}) depends on the original SOC and should approximately satisfy

$$\mathrm{SOC}\cdot E_{in} = c_{LIB} m_{LIB} (T_{max} - T_{re}) \tag{3}$$

where E_{in} is the internal energy release; m_{LIB} is the mass of the LIB; and $T_{re} \approx 90$ °C is the initiated temperature for self-heating reactions [47]. Based on the experimental data (Fig. 5c), the internal energy release of a 100% SOC LIB could be estimated as 682 kJ, which accounts for 88% of initial energy stored inside the cell. Therefore, only 12% of energy release during thermal runaway is removed by eruptions, verifying that the main heat transfer path for thermal runaway propagation of the large-format LIBs is the heat conduction though shells ($\dot{q}_s$) [26].

To simplify the problem and highlight the effect of firewalls, Eq. (2) can be simplified as

$$r = \frac{\text{Heating rate}}{\text{Necessary heat for TR}} \approx \frac{\dot{q}_s - \dot{q}_c}{m_{LIB} c_{LIB} (T_{crt} - T_0)} = \frac{\lambda_p (T_{max} - T_{crt}) A_s / \delta_p - h (T_{crt} - T_e) A_c}{m_{LIB} c_{LIB} (T_{crt} - T_0)} \tag{4}$$

where δ_p (mm) is the firewall plate thickness, λ_p (W/m-K) is its conductivity, A_s is the contact area between cells, A_c is the area of cell surface exposed to the environment, and h (W/m^2-K) is the overall heat transfer coefficient with the environment (T_e). Then, the thermal runaway propagation rate (r) decreases as the thickness of the HGM plate (δ_p) increases, as demonstrated in Fig. 8b. Thus, there should be a minimum thickness ($\delta_{p,min}$) to quench the thermal runaway propagation ($r = 0$) for this linear LIB module, as

$$\delta_{p,min} \geq \frac{\lambda_p (T_{max} - T_{crt}) A_s}{h (T_{crt} - T_e) A_c} \tag{5}$$

where the values of λ_p and h are key parameters for battery thermal management systems (BTMSs), A_s and A_c depend on the battery dimension, and characteristic temperatures of T_{max} and T_{crt} are related to the inherent safety properties of LIBs. Furthermore, a dimensionless number (Bi^*) can also be proposed to quantify the system performance in preventing thermal runaway propagation, which composes of the traditional Biot number $\frac{\delta_p/\lambda_p}{1/h}$ and the factor of the battery itself $\frac{(T_{crt}-T_e)A_c}{(T_{max}-T_{crt})A_s}$ as

$$Bi^* = \frac{\delta_p/\lambda_p}{1/h} \cdot \frac{(T_{crt} - T_e) A_c}{(T_{max} - T_{crt}) A_s} \geq 1 \tag{6}$$

The larger the value of Bi^*, the safer the battery module will be. Thus, this dimensionless number (Bi^*) could provide new insights into the safety design of the thermal management systems for the linear LIB modules. According to the characteristic temperatures of LIB in Fig. 7, the minimum thickness was calculated as 7 mm, which was 4 mm thicker than the HGM plate used in Fig. 7d. This is because the heat generation by failed battery are regarded as the heat sources for the adjacent cell, leading to the overestimation of the critical firewall thickness. From the perspective of safety design, a proper overestimation is considered acceptable.

The state-of-the-art BTMS should enhance the heat dissipation during the normal operating state of LIBs and facilitate thermal insulation when LIBs fail. However, the additional cooling systems and interstitial thermal barriers can reduce the energy density and increase the manufacturing costs. Based on Eq. (6), the synergistic relationship between thermal insulation (λ_p) and environmental heat exchange (h) can be optimized in a cost-effective way to achieve the thermal safety design for LIB modules ultimately.

4. Conclusions

In this work, the ultra-light HGM plates with low thermal conductivity are prepared for mitigating the thermal runaway propagation within high-energy LIB modules. The thermal, mechanical, and flame-retardant performances of prepared HGM plates are evaluated based on the standard tests. A series of experiments are conducted to investigate the effects of SOC and HGM plate thickness on thermal runaway propagation characteristics of NCM 811 LIB modules. Results indicate that the HGM plate with 60 wt.% HGM, 25 wt.% curing agent, and 15 wt.% flame retardants is the most suitable candidate for thermal runaway propagation prevention, exhibiting a low thermal conductivity of 0.064 W/(m-K), high compressive strength of 1.87 MPa, and can attain the UL 94V-0 flame-retardant standard.

Without firewalls, the intensive smoke emission and violent combustion are observed, and the toxic hazards of gas emissions are investigated with the aid of SEM/EDS analysis. As SOC increases from 25% to 100%, the thermal runaway propagation rate increases from 0.43 cell/min to 0.85 cell/min. However, inserting HGM plates can effectively impede TRP. The thermal runaway propagation rate over the fully charged LIB module decreases from 0.80 cell/min to 0 cell/min (no thermal runaway propagation occurrence) as the thickness increases of the HGM plate increases from 0 mm to 3 mm. Finally, a simplified heat transfer model is delivered to qualitatively elucidate the inhibition effect on thermal runaway propagation and guide the thermal safety design for LIB modules.

The thermal runaway propagation behaviors of large-format NCM 811 LIBs, especially for the characteristics of temperature evolution and venting particles, would be a significant addition to the current literature. The proposed passive strategies based on HGM plates could provide new insights to mitigate the thermal runaway propagation within LIB systems and have application prospects in safety engineering. Moreover, the simplified heat transfer model would help to evaluate the safety design of the LIB systems.

CRediT authorship contribution statement

Huichang Niu: Conceptualization, Methodology, Data curation, Investigation, Resources, Supervision, Writing - Original Draft. **Caixing Chen:** Methodology, Investigation. **Yanhui Liu:** Investigation, Writing - Original Draft, Formal analysis. **Lei Li:** Data curation. **Zhao Li:** Investigation. **Dan Ji:** Methodology, Resources. **Xinyan Huang:** Methodology, Funding acquisition, Supervision, Writing - Review & Editing.

Acknowledgments

This research is supported by the Hong Kong Research Grant Council through the Early Career Scheme (25205519), Shanghai Science and Technology Committee (19160760700), and Shenzhen Science and Technology Program (JCYJ20210324131006017).

References

[1] Liu J, Duan Q, Peng W, Feng L, Ma M, Hu S, et al. Slight overcharging cycling failure of commercial lithium-ion battery induced by the jelly roll destruction. *Process Safety and Environmental Protection* 2022;160:695–703.

[2] Lisbona D, Snee T. A review of hazards associated with primary lithium and lithium-ion batteries. *Process Safety and Environmental Protection* 2011;89:434–42.

[3] Wang Q, Mao B, Stoliarov SI, Sun J. A review of lithium ion battery failure mechanisms and fire prevention strategies. *Progress in Energy and Combustion Science* 2019;73:95–131.

[4] Feng X, Ren D, He X, Ouyang M. Mitigating Thermal Runaway of Lithium-Ion Batteries. *Joule* 2020;4:743–70.

[5] Vendra CMR, Shelke A V, Buston JEH, Gill J, Howard D, Read E, et al. Numerical and experimental characterisation of high energy density 21700 lithium-ion battery fires. *Process Safety and Environmental Protection* 2022;160:153–65.

[6] Sun P, Bisschop R, Niu H, Huang X. A Review of Battery Fires in Electric Vehicles. *Fire Technology* 2020;56:1361–1410.

[7] Yuan L, Dubaniewicz T, Zlochower I, Thomas R, Rayyan N. Experimental study on thermal runaway and vented gases of lithium-ion cells. *Process Safety and Environmental Protection* 2020;144:186–92.

[8] Bravo Diaz L, He X, Hu Z, Restuccia F, Marinescu M, Barreras JV, et al. Review—Meta-Review of Fire Safety of Lithium-Ion Batteries: Industry Challenges and Research Contributions. *Journal of The Electrochemical Society* 2020;167:090559.

[9] Liu Y, Niu H, Li Z, Liu J, Xu C, Huang X. Thermal runaway characteristics and failure criticality of massive ternary Li-ion battery piles in low-pressure storage and transport. *Process Safety and Environmental Protection* 2021;155:486–97.

[10] Yang Y-P, Jiang J-C, Huang A-C, Tang Y, Liu Y-C, Xie L-J, et al. 3-(Trifluoromethyl)benzoylacetonitrile: A multi-functional safe electrolyte additive for LiNi0.8Co0.1Mn0.1O2 cathode of high voltage lithium-ion battery. *Process Safety and Environmental Protection* 2022;160:80–90.

[11] Weng J, He Y, Ouyang D, Yang X, Chen M, Cui S, et al. Honeycomb-inspired design of a thermal management module and its mitigation effect on thermal runaway propagation. *Applied Thermal Engineering* 2021;195:117147.

[12] Dai X, Kong D, Du J, Zhang Y, Ping P. Investigation on effect of phase change material on the thermal runaway of lithium-ion battery and exploration of flame retardancy improvement. *Process Safety and Environmental Protection* 2022;159:232–42.

[13] Koch S, Birke KP, Kuhn R. Fast thermal runaway detection for lithium-ion cells in large scale traction batteries. *Batteries* 2018;4:16.

[14] Xiong R, Li L, Tian J. Towards a smarter battery management system: A critical review on battery state of health monitoring methods. *Journal of Power Sources* 2018;405:18–29.

[15] Liao Z, Zhang S, Li K, Zhang G, Habetler TG. A survey of methods for monitoring and detecting thermal runaway of lithium-ion batteries. *Journal of Power Sources* 2019;436:226879.

[16] Cai T, Valecha P, Tran V, Engle B, Stefanopoulou A, Siegel J. Detection of Li-ion battery failure and venting with Carbon Dioxide sensors. *ETransportation* 2021;7:100100.

[17] Lopez CF, Jeevarajan JA, Mukherjee PP. Experimental analysis of thermal runaway and propagation in

lithium-ion battery modules. *Journal of the Electrochemical Society* 2015;162:A1905–15.

[18] Larsson F, Anderson J, Andersson P, Mellander BE. Thermal modelling of cell-to-cell fire propagation and cascading thermal runaway failure effects for lithium-ion battery cells and modules using fire walls. *Journal of the Electrochemical Society* 2016.

[19] Weng J, Ouyang D, Liu Y, Chen M, Li Y, Huang X, et al. Alleviation on battery thermal runaway propagation: Effects of oxygen level and dilution gas. *Journal of Power Sources* 2021;509:230340.

[20] Yuan S, Chang C, Yan S, Zhou P, Qian X, Yuan M, et al. A review of fire-extinguishing agent on suppressing lithium-ion batteries fire. *Journal of Energy Chemistry* 2021;62:262–80.

[21] Liu Y, Yang K, Zhang M, Li S, Gao F, Duan Q, et al. The efficiency and toxicity of dodecafluoro-2-methylpentan-3-one in suppressing lithium-ion battery fire. *Journal of Energy Chemistry* 2022;65:532–40.

[22] Said AO, Stoliarov SI. Analysis of effectiveness of suppression of lithium ion battery fires with a clean agent. *Fire Safety Journal* 2021;121:103296.

[23] Liu T, Tao C, Wang X. Cooling control effect of water mist on thermal runaway propagation in lithium ion battery modules. *Applied Energy* 2020;267:115087.

[24] Xu J, Duan Q, Zhang L, Liu Y, Zhao C, Wang Q. Experimental study of the cooling effect of water mist on 18650 lithium-ion battery at different initial temperatures. *Process Safety and Environmental Protection* 2022;157:156–66.

[25] Liu P, Sun H, Qiao Y, Sun S, Wang C, Jin K, et al. Experimental study on the thermal runaway and fire behavior of LiNi0.8Co0.1Mn0.1O2 battery in open and confined spaces. *Process Safety and Environmental Protection* 2022;158:711–26.

[26] Feng X, Sun J, Ouyang M, Wang F, He X, Lu L, et al. Characterization of penetration induced thermal runaway propagation process within a large format lithium ion battery module. *Journal of Power Sources* 2015.

[27] Yuan C, Wang Q, Wang Y, Zhao Y. Inhibition effect of different interstitial materials on thermal runaway propagation in the cylindrical lithium-ion battery module. *Applied Thermal Engineering* 2019;153:39–50.

[28] Feng X, He X, Ouyang M, Lu L, Wu P, Kulp C, et al. Thermal runaway propagation model for designing a safer battery pack with 25Ah LiNixCoyMnzO2 large format lithium ion battery. *Applied Energy* 2015;154:74–91.

[29] Li L, Xu C, Chang R, Yang C, Jia C, Wang L, et al. Thermal-responsive, super-strong, ultrathin firewalls for quenching thermal runaway in high-energy battery modules. *Energy Storage Materials* 2021;40:329–36.

[30] Rui X, Feng X, Wang H, Yang H, Zhang Y, Wan M, et al. Synergistic effect of insulation and liquid cooling on mitigating the thermal runaway propagation in lithium-ion battery module. *Applied Thermal Engineering* 2021;199:117521.

[31] Niu J, Deng S, Gao X, Niu H, Fang Y, Zhang Z. Experimental study on low thermal conductive and flame retardant phase change composite material for mitigating battery thermal runaway propagation. *Journal of Energy Storage* 2022;47:103557.

[32] Weng J, Xiao C, Ouyang D, Yang X, Chen M, Zhang G, et al. Mitigation effects on thermal runaway propagation of structure-enhanced phase change material modules with flame retardant additives.

Energy 2022;239:122087.

[33] Hu Y, Mei R, An Z, Zhang J. Silicon rubber/hollow glass microsphere composites: Influence of broken hollow glass microsphere on mechanical and thermal insulation property. *Composites Science and Technology* 2013;79:64–9.

[34] Diallo AO, Len C, Morgan AB, Marlair G. Revisiting physico-chemical hazards of ionic liquids. *Separation and Purification Technology* 2012;97:228–34.

[35] Eshetu GG, Grugeon S, Laruelle S, Boyanov S, Lecocq A, Bertrand J-P, et al. In-depth safety-focused analysis of solvents used in electrolytes for large scale lithium ion batteries. *Physical Chemistry Chemical Physics* 2013;15:9145–55.

[36] Lecocq A, Eshetu GG, Grugeon S, Martin N, Laruelle S, Marlair G. Scenario-based prediction of Li-ion batteries fire-induced toxicity. *Journal of Power Sources* 2016;316:197–206.

[37] Wang W, He T, He S, You T, Khan F. Modeling of thermal runaway propagation of NMC battery packs after fast charging operation. *Process Safety and Environmental Protection* 2021;154:104–17.

[38] Mao B, Chen H, Jiang L, Zhao C, Sun J, Wang Q. Refined study on lithium ion battery combustion in open space and a combustion chamber. *Process Safety and Environmental Protection* 2020;139:133–46.

[39] Jin C, Sun Y, Wang H, Lai X, Wang S, Chen S, et al. Model and experiments to investigate thermal runaway characterization of lithium-ion batteries induced by external heating method. *Journal of Power Sources* 2021;504:230065.

[40] He X, Restuccia F, Zhang Y, Hu Z, Huang X, Fang J, et al. Experimental Study of Self-heating Ignition of Lithium-Ion Batteries During Storage: Effect of the Number of Cells. *Fire Technology* 2020;56:2649–69.

[41] Ouyang D, Weng J, Chen M, Wang J. What a role does the safety vent play in the safety of 18650-size lithium-ion batteries? *Process Safety and Environmental Protection* 2022;159:433–41.

[42] Niu H, Chen C, Ji D, Li L, Li Z, Liu Y, et al. Thermal-Runaway Propagation over a Linear Cylindrical Battery Module. *Fire Technology* 2020;56:2491–507.

[43] Li H, Duan Q, Zhao C, Huang Z, Wang Q. Experimental investigation on the thermal runaway and its propagation in the large format battery module with Li(Ni1/3Co1/3Mn1/3)O2 as cathode. *Journal of Hazardous Materials* 2019;375:241–54.

[44] Wang H, Du Z, Rui X, Wang S, Jin C, He L, et al. A comparative analysis on thermal runaway behavior of Li (NixCoyMnz) O2 battery with different nickel contents at cell and module level. *Journal of Hazardous Materials* 2020;393:122361.

[45] Zhang Y, Wang H, Li W, Li C. Quantitative identification of emissions from abused prismatic Ni-rich lithium-ion batteries. *ETransportation* 2019;2:100031.

[46] Ribière P, Grugeon S, Morcrette M, Boyanov S, Laruelle S, Marlair G. Investigation on the fire-induced hazards of Li-ion battery cells by fire calorimetry. *Energy & Environmental Science* 2012;5:5271.

[47] Wang Y, Ren D, Feng X, Wang L, Ouyang M. Thermal kinetics comparison of delithiated Li[NixCoyMn1-x-y]O2 cathodes. *Journal of Power Sources* 2021;514:230582.